POLITECNICO DI TORINO
Repository ISTITUZIONALE

Facile fabrication of shape memory poly(-caprolactone) non-woven mat by combining electrospinning and sol-gel reaction

(Article begins on next page)

14 October 2024

CrossMark
click for updates

Facile fabrication of shape memory poly(ε-caprolactone) non-woven mat by combining electrospinning and sol–gel reaction

Andrea Merlettini,[a] Stefano Pandini,*[b] Silvia Agnelli,[b] Chiara Gualandi,[a] Katia Paderni,[c] Massimo Messori,[c] Maurizio Toselli[d] and Maria Letizia Focarete*[a]

Poly(ε-caprolactone)-based non-woven fibrous mats showing excellent one-way shape memory properties were obtained through a straightforward approach by combining electrospinning process and sol–gel reaction. A solution of partially crosslinked α,ω-triethoxysilane-terminated poly(ε-caprolactone) was used to obtain bead-free fibers through electrospinning. Non-woven mats with different crosslinking degrees have been prepared and the effect of the different crosslinking extent and of the microfibrous structure were correlated to the mechanical and shape memory properties of the material. The evolution of fiber architecture within the non-woven mat following deformation and shape memory cycles was also investigated.

1. Introduction

Shape memory polymers (SMPs) are a class of smart materials able to interconvert between a "temporary" shape obtained after a programming step and a previously set "permanent" shape, upon the application of an external stimulus.[1] The most common SMPs belong to the class of the thermally induced shape memory (SM) materials.[2,3] In this case the polymer is able to recover its "permanent" shape just by heating the specimen at temperature above a transition temperature, T_{trans}, that is characteristic for each polymer. SMPs present interesting properties, such as good processability, low cost, the ability to recover very large strains and a relatively easy tailoring of the temperatures that trigger the shape memory effect.[4] A polymer exhibits a shape memory behaviour thanks to the presence of a suitable macromolecular network composed by net-points and molecular switches.[5] The former can be chemical (covalent bonds) or physical (intermolecular interactions), they are not destroyed by the temperature range required to express the shape memory behaviour and are responsible of the recovery of the permanent shape of the object. The molecular switches are the fractions of polymer chain that can be reversibly softened by temperature change. It is worth pointing out that SMPs

characterized by the presence of permanent chemical net-points will exhibit better shape memory performance than those with physical net-points, since the mechanical deformation may causes loss in physical crosslinks integrity.[6] Moreover, a fast and sharp shape recovery is exhibited when the external stimulus is efficiently distributed throughout the specimen.

Potential applications of SMPs exist in several sectors: self-repairing composites and textiles, sensors and biosensors, intelligent packaging and smart biomedical devices.[7] The latter represent one of the most interesting and attractive field in which biocompatible and biodegradable SMPs, whose transition temperature can be tuned to human body temperature or slightly above,[8,9] can be successfully applied. In this context, poly(ε-caprolactone) (PCL) is a particularly interesting polymer due to its biocompatibility and low melting temperature (T_m). Linear chain PCL alone is not a polymer able to express SM behavior due to the lack of a proper molecular network. A common approach is to prepare physically crosslinked copolymers where PCL crystal segments are the molecular switches that acquire mobility at a T_{trans} corresponding to the PCL T_m.[10–13]

Electrospinning technology[14] has been exploited to fabricate micro/nanofibrous matrices with SM properties,[15–19] that in some cases displayed an enhanced SM behaviour than the corresponding bulk films.[15] Promising biomedical applications of the electrospun SMPs can be found in the tissue engineering field, to control the cell behaviour through mechanical–biological stimuli[16] and in regenerative medicine to assist bone growth.[17]

Matsumoto and coworkers[18] explored the SM capability of electrospun non-woven mat of a multiblock copolymer consisting of crystallizable poly(ω-pentadecalactone) hard

[a]Department of Chemistry "G. Ciamician" and INSTM UdR of Bologna, University of Bologna, Via Selmi 2, 40126 Bologna, Italy. E-mail: marialetizia.focarete@unibo.it
[b]Department of Mechanical and Industrial Engineering of Brescia, University of Brescia, Via Branze 38, 25123 Brescia, Italy. E-mail: stefano.pandini@unibs.it
[c]Department of Engineering "E. Ferrari" and INSTM Udr of Modena and Reggio Emilia, University of Modena and Reggio Emilia, Via P. Vivarelli 10/1, 41125 Modena, Italy
[d]Department of Industrial Chemistry "Toso Montanari", University of Bologna, Viale Risorgimento 4, 40136 Bologna, Italy

segments, acting as physical crosslinks, and PCL switching segments. Only few works report the production of SM fibrous mat based on plain PCL and in these cases a crosslinking treatment of the polymeric fibrous matrix is always needed. Gong *et al.*[19] produced SM PCL mats reinforced with multi-walled carbon nanotubes (MWNTs) and coated with Fe_3O_4 to obtain a material with a shape memory effect, triggered both by hot water and by the exposure to a specific magnetic field. The chemical crosslinking was carried out under ultraviolet irradiation during the electrospinning process, obtaining a SMP with gel content (G) of less than 50% with promising SM behaviour. Chen *et al.*[15] produced a crosslinked SM mat starting from a γ-aminopropyltriethoxysilane end-capped polyurethane oligomer containing a block of PCL that was partially hydrolyzed and condensed through the ethoxysilane groups before electrospinning. However, to get an electro-spinnable solution providing bead-free fibers they added pol-yvinylpyrrolidone as a template material during the electrospinning process, that was later removed after cross-linking the electrospun mat. To prevent the fibers to stick together they immersed the mat in liquid paraffin in order to be able to perform a post-crosslinking treatment without affecting the micro/nanofibrous structure.

In order to obtain electrospun mats with good SM properties and to overcome the limitations of complex approaches inves-tigated in literature up to now, in this work we propose a novel and straightforward approach by combining electrospinning process and sol–gel reaction that enabled to achieve high crosslinking degrees without using any template polymer. This new approach, that is based on the combination of electro-spinning with another technology, contributes to go beyond the simple one-step process and expands the electrospinning capability of creating nanoproducts, similarly to other electro-spinning technological modifications previously proposed.[20–22] A partially crosslinked PCL, synthesized through sol–gel chemistry starting from a α,ω-triethoxysilane-terminated PCL,[23] was used to gain bead-free fibers. After electrospinning, the crosslinking degree has been subsequently increased and tuned by applying a controlled thermal treatment. Electrospun samples with different crosslinking degrees have been prepared and the effect of the different crosslinking extent was correlated to the SM property of the material by applying an *ad hoc* ther-momechanical cycle. Furthermore, gel content, degree of swelling and morphology of the samples have been studied. The obtained shape memory mats might have useful applications in the biomedical field.

2. Materials and methods

2.1 Materials

α,ω-Hydroxyl-terminated poly(ε-caprolactone) (average $M_n \sim$ 10 000 g mol^{-1} and average $M_w \sim$ 14 000 g mol^{-1}), 3-(triethox-ysilyl)propyl isocyanate (ICPTS), tetrahydrofuran (THF), chlo-roform, *N,N*-dimethylformamide (DMF) and hydrochloric acid (37% w/w in H_2O) were purchased from Sigma-Aldrich and used as received without any further purification.

2.2 Synthesis of α,ω-triethoxysilane-terminated poly(ε-caprolactone)

α,ω-Hydroxyl-terminated PCL was dried overnight at 55 °C under dynamic vacuum in the presence of molecular sieves just before reaction with ICPTS. α,ω-Triethoxysilane-terminated PCL was prepared by introducing dried hydroxyl-terminated polyester and ICPTS into a glass flask, previously flushed three times with cycles of vacuum-nitrogen. The reaction was carried out in bulk at 130 °C for 2 h under nitrogen atmosphere and magnetic stirring. ICPTS was added with a 20% stoichio-metric excess with respect to hydroxyl groups of PCL. Unreacted ICPTS was removed by dynamic vacuum at the end of the reaction. More details concerning the preparation and the characterization of α,ω-triethoxysilane-terminated PCL are re-ported in a previous paper.[23]

2.3 Sol–gel electrospinning

α,ω-Triethoxysilane-terminated PCL was dissolved at a concen-tration of 35% w/v in THF : DMF = 80 : 20 (v/v). Water (for the hydrolysis reaction) and HCl (as catalyst) were added at the following molar ratios (with respect to ethoxide groups of the α,ω-triethoxysilane-terminated PCL): EtO : H_2O : HCl = 1 : 0.5 : 0.005 corresponding to 0.54% w/w of water and 0.011% w/w of HCl with respect to the polymer weight. The sol–gel solution was stirred for 17 h in a sealed glove box at 19 °C and 40% of relative humidity (RH). The solution was then trans-ferred to the syringe and electrospun by means of a homemade electrospinning apparatus, comprised of a high-voltage power supply (Spellman SL 50 P 10/CE/230), a syringe pump (KD Scientific 200 series), a glass syringe, a stainless steel blunt-ended needle (inner diameter = 0.31 mm) connected with the power supply electrode (ΔV = 17 kV), and a grounded aluminium drum-type collector (diameter 5 cm) rotating at 100 rpm. Polymer solution was dispensed with a flow rate of 0.6 mL h^{-1} through a Teflon tube to the needle which was placed vertically on the collecting drum at a distance of 25 cm. The electrospun mats were produced at room temperature (RT) and at RH = 50%.

2.4 Post-crosslinking

The post-crosslinking treatment was performed by storing the electrospun mat in an oven (Binder, Germany), in the presence of acid environment, at 50 °C for either 3 h or 72 h to obtain post-crosslinked PCL with a low and high crosslinking degree, respectively. The samples were thus labelled PCL-low and PCL-high, accordingly. The electrospun mat was hanged to a glass rod at the top of a 500 mL beaker. The beaker was filled with 100 mL of distilled water and 3 mL of HCl 37%. The electrospun mat was not in direct contact with the acid solution but only with its acidic vapours.

2.5 Gel content and degree of swelling

Specimens of as-spun and post-crosslinked non-wovens (20 × 20 × ~0.1 mm^3) were weighed to get their initial weight (m_0) and then immersed in 15 mL of THF overnight. After 17 h the

THF was replaced with fresh THF. After stirring for 2 h the excess of THF was removed from the samples and they were weighted to record the mass of the swollen sample (m_s). Subsequently, the swollen samples were laid in a Petri dish and dried at RT overnight in order to determine the residual mass (m_d) after dissolution of non-crosslinked PCL macromolecules in THF. The degree of swelling of the crosslinked polymer (Q) and the gel content (G) were calculated according to eqn (2.1) and (2.2), respectively:

$$Q = \frac{V_s}{V_d} = 1 + \frac{\rho_2}{\rho_1}\left(\frac{m_s}{m_d} - 1\right) \tag{2.1}$$

$$G = \frac{m_d}{m_0} \times 100 \tag{2.2}$$

where V_s is the volume of the swollen mat, V_d is the volume of the dried mat, ρ_1 is the THF density (0.889 g cm^{-3}) and ρ_2 is the PCL density (1.094 g cm^{-3}).

2.6 Thermo-mechanical characterization

2.6.1 Specimens preparation. The thermo-mechanical and shape memory tests were carried out on specimens of the two post-crosslinked electrospun mats. The specimens were cut as rectangular strips (overall length: 30 mm; width: 0.5 mm) from the electrospun mat and required a preliminary thermal treatment to achieve dimensional stability. In fact, the specimens obtained by means of electrospinning and subsequent post-crosslinking, still present significant shrinkage effects, probably as a consequence of the high stretching of the fibers. Before and after the thermal treatment the width of the specimens was determined by means of an optical travelling microscope, while the thickness was determined by means of a digital micrometer. Shrinking effects are activated by heating the material slightly above T_m and usually determine a contraction of about 30–35% of the specimen width and length, and a thickness increase of about 50%. In presence of such dimensional variations a proper evaluation of the shape memory response may be prohibited, due to overlapping of the shrinkage and shape memory effects. Therefore, before the shape memory characterization, all the specimens were preliminary subjected to a thermal treatment that allows the free shrinkage of the specimen and consisting in heating the specimen at 85 °C (*i.e.* well above melting temperature), maintaining this temperature for 15 min, and later cooling the specimen to 0 °C. Such preparation protocol allowed to provide good dimensional stability to the specimens, which, as experimentally verified, will not undergo any other dimensional change except for thermal contraction/expansion when cooled/heated at a temperature different than RT. In the thermo-mechanical and shape memory tests, the data were treated on the basis of the dimensions of the shrunk specimens.

2.6.2 DMTA analysis. The dynamic mechanical thermal analysis (DMTA) of the materials was carried out on the thermally treated strips (gauge length: 10 mm) by means of a dynamic mechanical analyzer (DMA Q800; TA Instruments), under a tensile configuration. The specimens were tested within a heating ramp from 23 °C to 75 °C at 1 °C min^{-1}, adopting a frequency of 1 Hz and under displacement control;

a moderate value of displacement amplitude was kept up to about 58 °C (15 μm for PCL-high, and 50 μm for PCL-low), raising it to higher values at higher temperatures (70 μm for PCL-high, and 150 μm for PCL-low); this was done in order to obtain reliable data up to the temperature above T_m, since the specimens became very compliant upon melting.

The mechanical behaviour of the materials was further explored in tensile tests carried out at 80 °C, *i.e.* at the temperature at which the specimens were deformed in the one-way shape memory tests on rectangular strips (average gauge length: 7 mm). The tests, performed by means of the DMA Q800, were carried out as a tensile ramp under load control at 0.05 N min^{-1}, after having equilibrated the specimens for 10 min at 80 °C. The output of the test was the stress *vs.* strain relationship for the systems investigated. It has to be remarked that the values of stress and strain here evaluated refer to the overall macro-mechanical behaviour of the fibrous microporous systems; further the values of stresses have to be taken into account as approximate results, due to the difficulties in determining a correct value of thickness by means of the digital micrometer. Tensile stress and strain were evaluated as engineering values according to the eqn (2.3) and (2.4):

$$\sigma = \frac{F}{A_0} \tag{2.3}$$

$$\varepsilon = \frac{\Delta l}{l_0} \tag{2.4}$$

where F represents the load; Δl is the DMA crosshead displacement; A_0 and l_0 are the overall specimen initial cross-section and the distance between clamps, respectively. The modulus was evaluated as the slope of the initial linear trend of the stress *vs.* strain curve.

2.6.3 One-way shape memory tests. Thermo-mechanical cycles were carried out on the thermally treated material to investigate its one-way shape memory behaviour. The tests were carried out on rectangular strips (average overall length: 20 mm; average gauge length: 7 mm; average cross-section: 0.5 mm^2) by employing the DMA under tensile configuration. A traditional shape memory cyclic history was adopted, consisting in the following steps: (i) heating the specimen up to 80 °C, *i.e.* above the polymer T_m; (ii) deforming the specimen at 80 °C up to a given level of strain, ε_{appl}, ranging between about 25% to about 200%, under load control (loading rate: 0.05 N min^{-1}); (iii) cooling the specimen under fixed strain condition to 0 °C, *i.e.* below the polymer crystallization temperature (T_c), and then unloading; (iv) monitoring the strain recovery during a heating ramp at 2 °C min^{-1} up to 80 °C. During the heating step (i) and recovery step (iv) the specimen was maintained under a constant load of 0.005 N. This load was necessary to maintain the specimen in tension during the heating ramps, to monitor its quasi stress-free strain changes and to avoid buckling and wrinkles; nevertheless, due to its moderate entity, also creep effects were avoided. Anyway the presence of this load exerts a pre-strain on the specimen, which has to be considered as the initial condition of the shape memory cycle; this pre-strain, ε_0, is found at the end of step (i), after equilibrating the specimen

at 80 °C for 5 minutes, and generally ranges between about 1% and 7%. The one-way shape memory capabilities were described in terms of strain fixity, which quantifies the amount of the applied strain fixed at the end of the cooling step, and strain recovery, representing the amount of applied strain recovered by the specimen by heating up to above T_m, and thus the ability to recover to its pristine strain, ε_0. These parameters are evaluated as follows:

$$\text{Strain fixity } (\%) = R_f = \frac{\varepsilon_{unload}}{\varepsilon_{applied}} \times 100 \qquad (2.5)$$

where ε_{appl} is the applied deformation (end of step ii) and ε_{unload} is the strain after load removal (end of step iii).

$$\text{Strain recovery } (\%) = R_r = \frac{\varepsilon_{applied} - \varepsilon_{rec}}{\varepsilon_{applied} - \varepsilon_0} \times 100 \qquad (2.6)$$

where ε_{rec} is the residual strain measured after the heating ramp (end of step iv), and we recall, ε_0, as the pre-strain measured before deformation (end of step i). Particular attention was reserved to evaluate the material cyclic recovery ability, and, on the more crosslinked mat (PCL-high), the shape memory cycle was carried out at least twice, and for a strain of about 100%, also a five-fold one-way thermo-mechanical history was applied; the strain fixity and strain recovery were determined for each cycle, taking as reference strain for the undeformed specimen the pre-strain ε_0 measured at the end of the first heating.

2.7 Other characterization techniques

Rheology experiments were carried out on an Anton Paar Rheometer MCR 102 using a cone-plate configuration (50 mm diameter, 1°). Experiments were performed at constant temperature of 19 °C controlled by the integrated Peltier system and a Julabo AWC100 cooling system. To prevent solvent evaporation a solvent trap (H-PTD200) was used. The flow curves were acquired at shear rate (γ) ranging from 0.1 s^{-1} to 100 s^{-1}.

Thermal characterization of the electrospun mat was carried out by means of differential scanning calorimetry (DSC Q100; TA Instruments), on about 5 mg sample cut from the thermally treated specimens. The thermal program employed consisted in a first heating from −90 °C to 100 °C at a heating rate of 10 °C min^{-1}, followed by cooling to −90 °C at 10 °C min^{-1}, and to a subsequent heating up to 100 °C at 10 °C min^{-1}. The DSC traces allowed to evaluate the glass transition temperature, T_g, the T_c, as the exothermal peak temperature of the cooling run, and the T_m, as the peak of the endothermal peak of the second heating run; from this latter curve also, the heat of fusion (ΔH_m) was determined, and the crystallinity content was evaluated by considering the ΔH_m of a 100% crystalline PCL of 134.9 J g^{-1}.[24]

Fiber morphology was investigated by scanning electron microscopy (SEM), employing a Cambridge S260 microscope. The analysis was carried out on as-spun mat as well as on post-crosslinked mats and on mats subjected to deformation and to shape memory history. In particular, the latter were studied under three specific conditions: (i) undeformed; (ii) deformed at various strain levels; (iii) at the end of a shape memory cycle. The SEM analysis on the undeformed mat was taken on a specimen after the preliminary thermal treatment. The morphology of the deformed systems was investigated through an *ex situ* analysis carried out on specimens deformed at 80 °C and at given levels of strain (25%; 50%; 100%; 185%) and cooled under fixed strain conditions at 0 °C to fix this temporary deformation. The specimens at the end of a single and of a five-fold shape memory cycle were cooled to 0 °C to fix the system morphology at the end of the strain recovery step. The specimens were kept in the refrigerator at −15 °C prior to the observation and sputtered with gold before the SEM analysis. The morphology was described in terms of fiber alignment, evaluated through two-dimensional fast Fourier transform (2D FFT) image analysis.[16,25] A 760 × 760 pixel square area was selected on the SEM image and analyzed by means of the software ImageJ 1.47V, using the FFT function and, subsequently, the "Oval Profile" plugin on a circular area (diameter: 760 pixel). This allowed to estimate pixel intensity along radii oriented at various angles, varying from 0° to 359°, summing the intensity along each radius and normalizing it by the minimum intensity value.

3. Results and discussion

SMP based on PCL should present a non-reversible covalent crosslink network that, in this work, was achieved by exploiting the reactive terminals of a previously synthesized α,ω-triethoxysilane-terminated PCL. The density of the reactive terminals is directly correlated to the molecular weight of the starting material, and thus a more crosslinked system can be more easily achieved by starting from a low molecular weight α,ω-triethoxysilane-terminated PCL rather than from a high molecular weight α,ω-triethoxysilane-terminated PCL. On the other hand it is well known that an efficient electrospinning process is usually obtained with high molecular weight polymers. Considering these two opposite aspects an α,ω-hydroxyl PCL with M_n of about 10 000 g mol^{-1} was used. Indeed this polymer was characterized by the highest molecular weight among the previously synthesized ones[23] and, after sol–gel crosslinking, exhibited a promising SM behavior in bulk state, *i.e.* the number of reactive terminals of the polymer was high enough to create a covalent net-point network featuring shape memory capabilities.[23]

Preliminary experiments to produce non-woven fibrous mats property consisted in electrospinning solutions of not-crosslinked α,ω-triethoxysilane-terminated PCL in THF : DMF = 80 : 20 (v/v) at increasing polymer concentration. All the performed experiments resulted in the collection of polymeric beads rather than fibers (see Fig. 1A as an example). It is well known that solution viscosity, determined by polymer molecular weight and polymer concentration, is the key parameter that defines polymer processability into continuous fibers through electrospinning. Indeed, it was demonstrated that chain entanglement concentration is the main parameter that influence fiber formation during electrospinning[26] for a specific polymer with a defined molecular weight, and the minimum concentration at which a polymer can produce uniform fibers is related to the entanglement density of the polymer solution.[26–29]
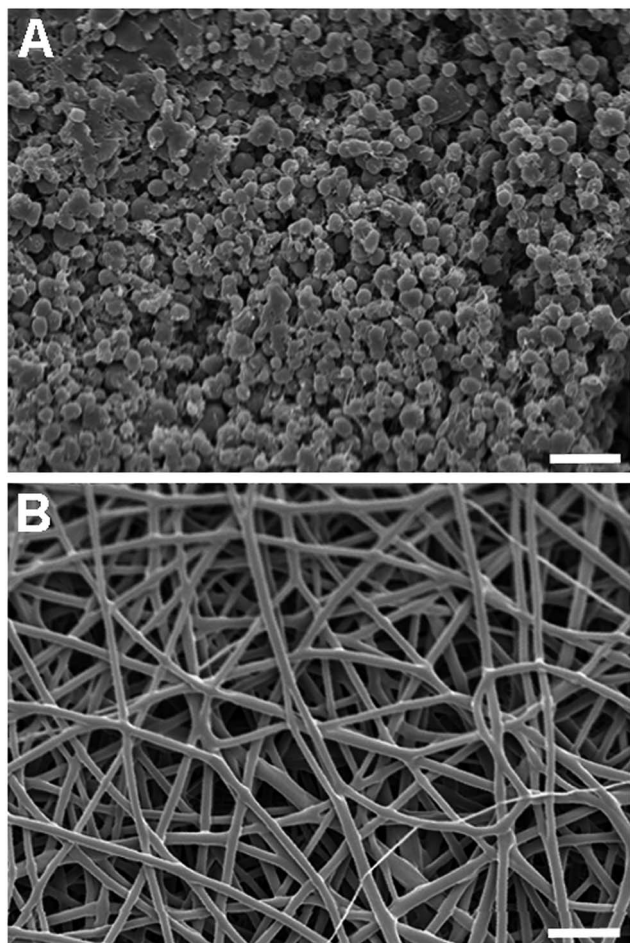
Fig. 1 SEM images of the electrospun meshes obtained from (A) 35% w/v α,ω-triethoxysilane-terminated PCL solution in THF : DMF = 80 : 20 (v/v) and (B) 35% w/v α,ω-triethoxysilane-terminated PCL solution in THF : DMF = 80 : 20 (v/v) with the addition of H_2O and HCl (sol−gel solution). Scale bars = 20 μm.

In the presence of elastically deformable entanglement network obtained above a critical polymer concentration and/or polymer molecular weight, viscoelastic forces are high enough to allow the generation of continuous fibers and the polymer is collected in the form of bead-free fibers. In the case of our polymeric system, with the aim of increasing entanglement density and hence solution viscosity, the reactive triethoxysilane terminal groups have been activated by adding to the polymer solution water and HCl (as indicated in the Materials and methods section). The resultant sol–gel solution of α,ω-triethoxysilane-terminated PCL was electrospun and continuous bead-free fibers were obtained (Fig. 1B). It is worth noting that by further increasing the amount of water and HCl the polymer solution turned into a gel after few hours of stirring and electrospinning was not possible. The dramatic change of morphology, from polymer beads into continuous fibers achieved by the addition of a low amount of water and acid can be explained by the occurrence, in the sol–gel solution, of a partial crosslinking reaction before electrospinning process (herein defined pre-crosslinking), schematically represented in Fig. 2A.

The pre-crosslinking led to the formation of Si–O–Si linkages between polymer chains, as a consequence of hydrolysis of the triethoxysilane terminal groups and their condensation, and therefore to an increase of PCL molecular weight, thus obtaining an electrospinnable solution (Fig. 2B) that provided bead-free fibers (Fig. 1B).

Rheological analysis was performed to verify that the change of electrospun polymer morphology from beads to defect-free fibers (Fig. 1) was related to a change of solution viscosity. The viscosity of the formulation that led to bead-free fibers after several hours of stirring was monitored at different times after solution preparation (Fig. 3). The viscosity of the solution, initially too low to provide bead-free fibers, slightly increased during the first hour of stirring at RT (from 0.032 Pa s to 0.034 Pa s, Fig. 3, curve A and B) and rapidly increased after 2 hours (0.065 Pa s, Fig. 3, curve D), reaching a value of 0.11 Pa s after 17 hours of stirring (Fig. 3, curve E) when an electrospinnable solution, that led to a bead-free electrospun mat, was obtained. As already mentioned, by increasing the water and acid concentration, the solution turned into a not electrospinnable gel in few hours. Therefore, the use of small amounts of H_2O and HCl activated only a fraction of triethoxysilane reactive terminals for the generation of a limited number of Si–O–Si covalent bond. The α,ω-triethoxysilane-terminated PCL electrospun mat was thus subjected to a post-crosslinking treatment (Fig. 2C) in order to increase the net-points density between the macromolecular chains. The post-crosslinking treatment was performed by exposing the mats to acid aqueous vapours that induced the formation of further Si–O–Si covalent bonds to generate a 3D network of PCL macromolecules. It is known that hydrolysis and condensation reactions are accelerated by increasing the temperature. However, for not compromising the morphology of the obtained fibers the post-crosslinking treatment had to be carried out at a temperature below polymer T_m. DSC analysis of the partially crosslinked electrospun α,ω-triethoxysilane-terminated PCL showed a T_g around −60 °C and a broad endotherm in the temperature range 40–70 °C, with a maximum peak around 55 °C (T_m).

Electrospun mats were kept at different temperatures (below PCL T_m) in order to determine the highest one that enables the maintenance of fiber morphology for the successive post-crosslinking treatments. In Fig. 4 SEM images of the electrospun PCL samples stored at different temperatures (45 °C and 50 °C) for 1 h are reported, revealing that both the investigated temperatures caused a small increase of fibers diameter from around 1.8 μm to around 2.2 μm. Furthermore it is pointed out that the mat stored at 50 °C underwent a small macroscopic shrinkage due to the melting of a small fraction of polymer crystal phase (in accordance with DSC results), thus no higher temperatures were tested and 50 °C was selected as the operating temperature for the post-crosslinking treatments.

Post-crosslinking was carried out by keeping the electrospun samples at 50 °C either for 3 h or 72 h, in order to achieve two different crosslinking degrees that were subsequently quantified in terms of degree of swelling (Q) in THF and gel content (G) according to eqn (2.1) and (2.2). Q and G of the starting electrospun mat were also determined for comparison. The mats
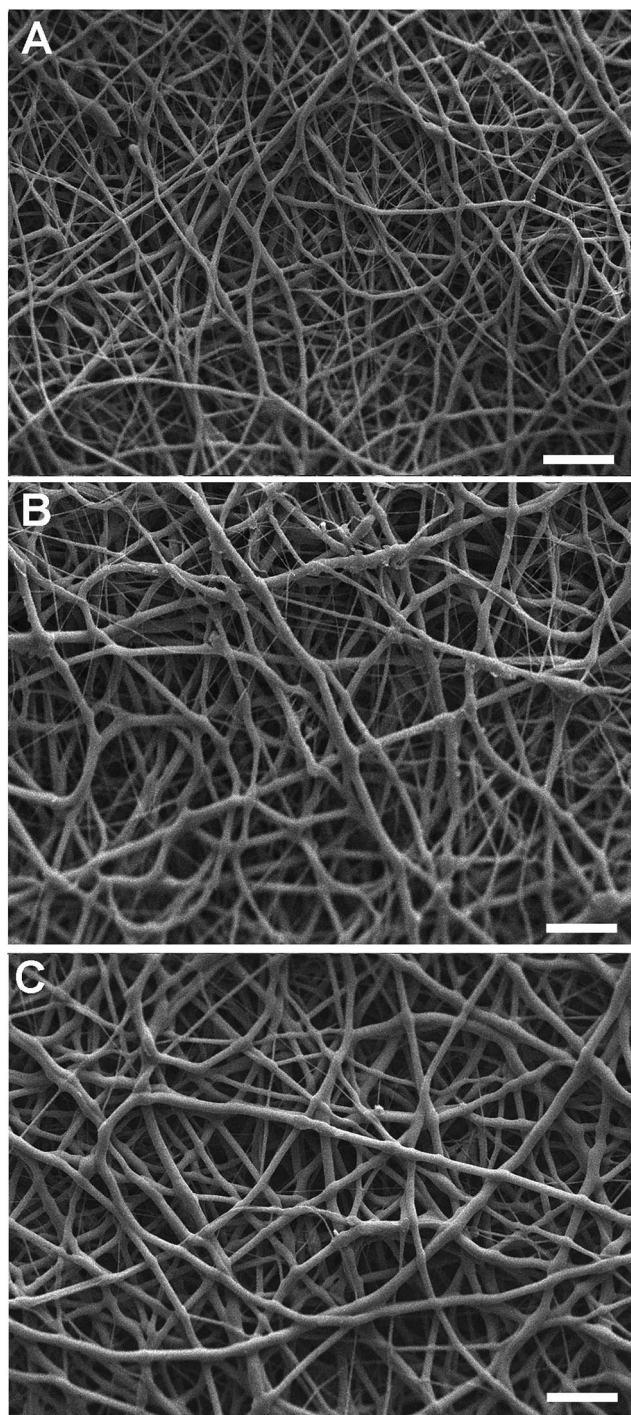
Fig. 2 (A) Pre-crosslinking: α,ω-triethoxysilane-terminated PCL solution was subjected to a partial sol–gel reaction to increase polymer molecular weight, due to the formation of Si–O–Si crosslink points. (B) Electrospinning: the pre-crosslinked solution was electrospun to obtain partially crosslinked fibers. (C) Post-crosslinking: the attained electrospun mat was subsequently thermally post-crosslinked achieving a semicrystalline crosslinked electrospun shape memory polymer.

immersed in THF are expected to swell to a certain extent, according to their crosslink density. Concomitantly, the macromolecular chains not involved in the molecular network dissolve in THF. Therefore, with the increase of crosslinking degree the Q value is expected to decrease while the G value is expected to increase. The values reported in Table 1 confirm the

Fig. 3 Flow curves of 35% w/v α,ω-triethoxysilane-terminated PCL in THF : DMF = 80 : 20 sol–gel solution acquired during the partial pre-crosslinking treatment at different times at RT. (A) $t = 0'$ (B) $t = 60'$ (C) $t = 100'$ (D) $t = 120'$ (E) $t = 17$ h.

expected increase of crosslinking density after post-crosslinking treatments. Indeed, after 3 h and 72 h at 50 °C, the G value of the as-spun PCL mat increased from 33.4% to 60% and 81.4%, respectively, while Q values decreased from 44 v/v to 5 v/v and 1.54 v/v, respectively.

The thermal properties of the post-crosslinked electrospun mats with two different crosslinking degrees were investigated through DSC test. Both PCL-low and PCL-high showed a T_g located at −60 °C, T_m at 55 °C and a T_c at 31 °C; further, a high crystallinity content of about 41% was estimated from the heat of fusion of the second heating scan, accordingly with the previously obtained results in bulk state starting from PCL precursors with the same molecular weight.[30]

The dynamic mechanical response of the mats, investigated in DMA tests from RT to above T_m, is reported in terms of the storage modulus trace in Fig. 5A. The electrospun mats having two different crosslinking degrees show a very similar behaviour, with storage modulus values in the order of tens of MPa at RT, and approaching a drop of about two orders of magnitude when crossing the T_m. At higher temperatures, thanks to the crosslinked structure, a plateau is approached, at about 200 kPa for PCL-high and, as expected, at a slightly lower value for PCL-low.

The mechanical behaviour in the rubbery plateau region was investigated in tensile tests performed at 80 °C. The stress *vs.* strain relationship measured at this temperature was needed to evaluate the material behaviour in the deformation ramp of the shape memory cycle, and more specifically to evaluate the maximum strain that can be applied in a shape memory test. The results are reported in Fig. 5B. A tensile modulus of (320 ± 30) kPa was measured for PCL-high and (200 ± 40) kPa for PCL-low. A highly ductile behavior was shown by both mats, and when subjected to deformations of about 200% the specimen never displayed failure.

The evolution of the microstructure with strain, for a deformation carried out in the rubbery-like region, was investigated, on PCL-high, by means of an *ex situ* SEM analysis of specimens deformed at various strain levels and fixed at the applied strain,

Fig. 4 SEM images of the electrospun PCL mat at (A) RT, (B) after 1 h at 45 °C and (C) after 1 h at 50 °C. Scale bars = 20 μm.

Table 1 Degree of swelling (Q) and gel content (G) of the as-spun and post-crosslinked PCL mats

Sample	Q^a (v/v)	G^b (%)
As-spun PCL	44 ± 5	33.4 ± 0.6
PCL-low	5.0 ± 0.3	60.0 ± 0.4
PCL-high	1.54 ± 0.06	81.4 ± 0.2

^{a} Calculated according to eqn (2.1). ^{b} Calculated according to eqn (2.2).
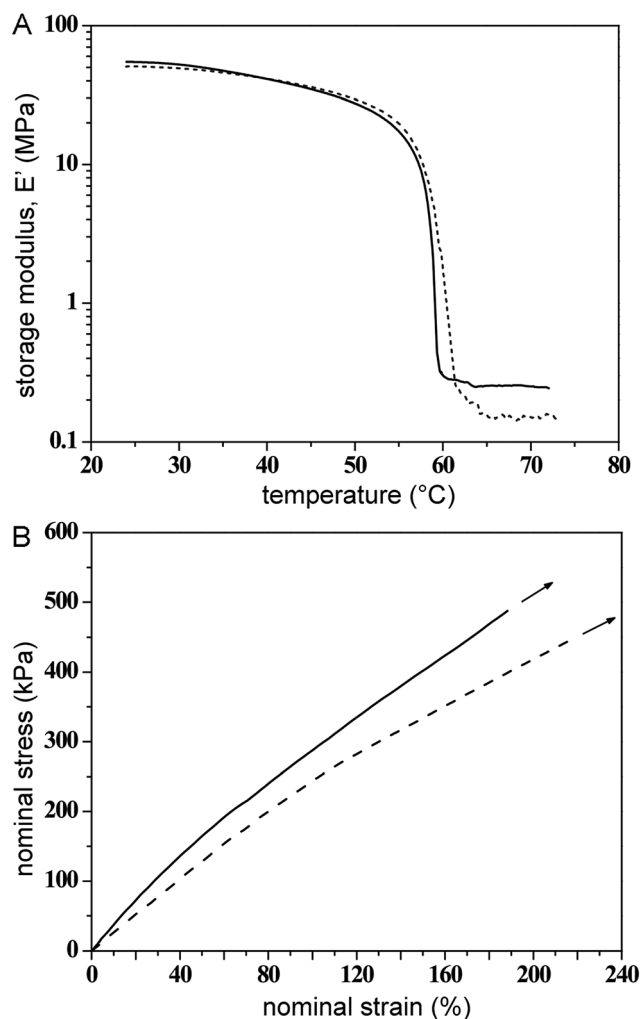
Fig. 5 Thermo-mechanical properties in terms of storage modulus trace as a function of temperature (A) and of stress vs. strain curves above T_m (B) for PCL-high (continuous line) and for PCL-low (dashed line); the arrows are reported to indicate that the specimens did not break and may be further deformed.

ε_{appl}, by means of cooling below T_c under fixed strain conditions. The good fixing capabilities, as it will be discussed later, allow to refer to the actual specimen strain practically as to the applied strain value. The results are reported in Fig. 6, comparing the morphology of an undeformed specimen (Fig. 6A) with that of various levels of strain (25%; 50%; 100%; 185%; Fig. 6B–E, respectively). A significant evolution of fiber architecture with the applied strain is highlighted, mainly consisting in a more pronounced alignment along the deformation direction as the strain increases. In particular, for strain levels above 50% the fibers show to be highly stretched and aligned along strain direction. To better highlight the alignment degree the images are accompanied by 2-D fast Fourier transform (2-D FFT) plots (Fig. 6F), representing the normalized intensity of the pixel along specific direction (0° representing a direction perpendicular to that of deformation). The curve of
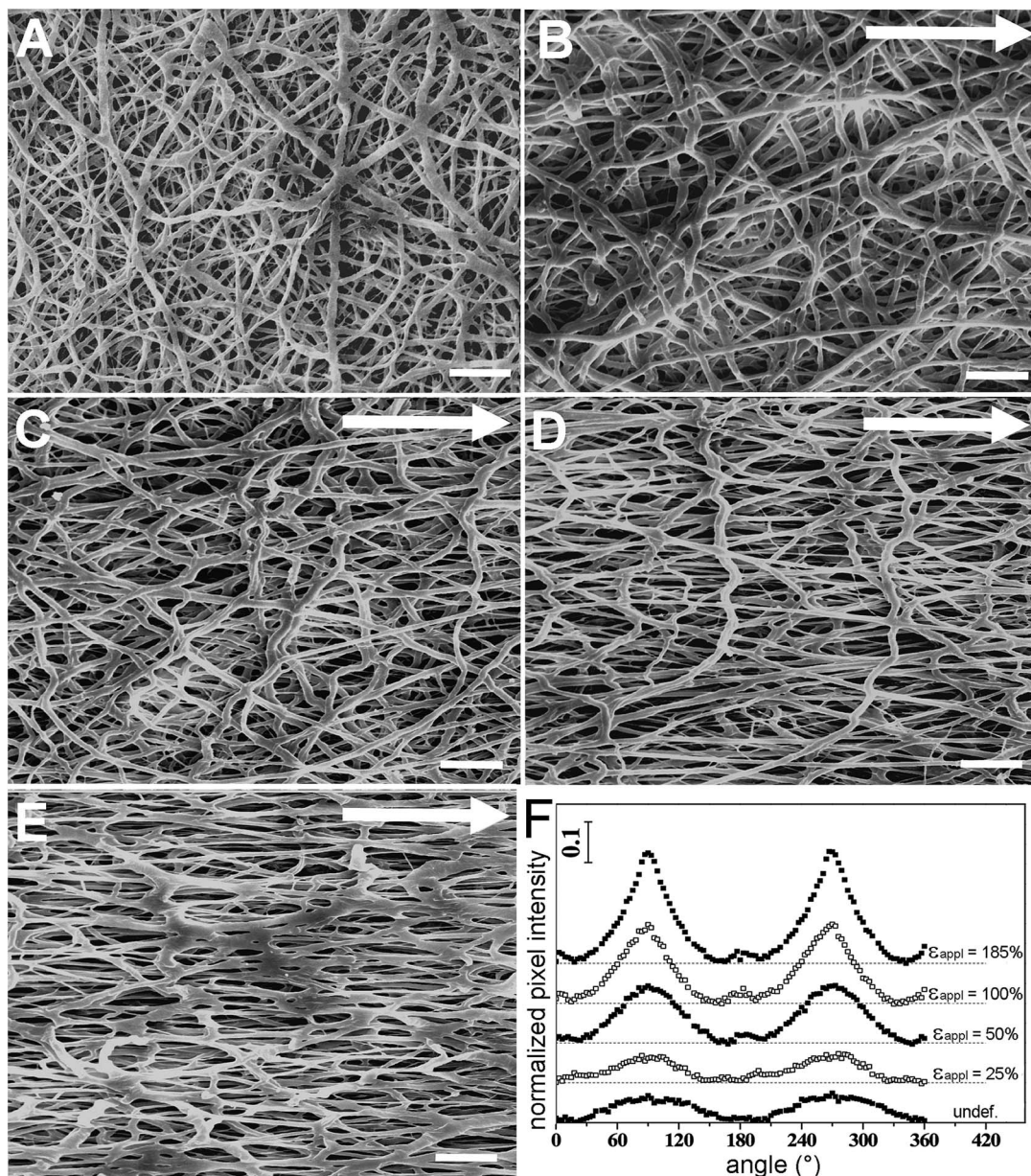
Fig. 6 Images from the *ex situ* SEM analysis carried out on PCL-high. Figures refer to an undeformed specimen (A) and deformed at progressively higher strain levels ((B) 25%; (C) 50%; (D) 100%; (E) 185%), the strain direction (indicated by the arrow) being parallel with the major length of the image; (F) 2-D FFT frequency distributions of the corresponding SEM images (curves vertically shifted of an arbitrary quantity to improve readability). Scale bars = 20 μm.

the undeformed specimen, which shows two broad peaks can be considered as a reference curve for the pristine randomly oriented state. The more pronounced fibers alignment is clearly evidenced by the peaks at 90° and 270° which become more intense and narrower for strain levels above 25%. The progressive orientation along the strain direction occurs at first prevalently through rotational/flexural rearrangements of the fibers (Fig. 6B and C), which start to be effectively stretched at nominal strain above 50% (Fig. 6D and E). At the highest level of nominal strain explored (Fig. 6E) the stretching of the fiber networks becomes particularly relevant, as testified by the highly deformed appearance of the region on which the fibers

overlap, as already shown in highly stretched non-woven membranes.[31] This latter image indicates a significant fiber–fiber cohesion, presumably achieved during the processing and thermal history of the specimen, through post-crosslinking or local melting.[32,33] Further it is shown that, on a micromechanical point of view, the mats undergo important morphological changes with strain, evolving from the structure of a material governed by the fiber rearrangements to practically that of a highly porous material.

The shape memory performances of the electrospun mats were investigated by means of a conventional one-way cyclic shape memory testing methodology, and a representation of the
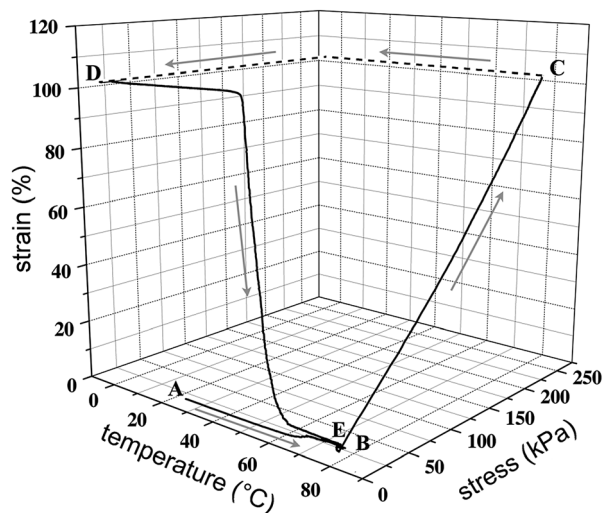
Fig. 7 Thermo-mechanical history for a one-way shape memory cycle for $\varepsilon_{appl} = 102\%$ ((A and B) heating; (B and C) deformation; (C and D) cooling under fixed strain and unloading; (D and E) quasi stress-free recovery); cycle carried out on PCL-high.

Table 2 Strain fixity and strain recovery capabilities for different values of applied strain and after various shape memory cycles applied to PCL-high

ε_{appl} (%)	1st cycle		2nd cycle		5th cycle	
	$R_f{}^a$ (%)	$R_r{}^b$ (%)	$R_f{}^a$ (%)	$R_r{}^b$ (%)	$R_f{}^a$ (%)	$R_r{}^b$ (%)
24	100	100	100	100	—	—
55	100	98	100	98	—	—
106	100	98	100	99	100	99

^{a} Calculated according to eqn (2.5). ^{b} Calculated according to eqn (2.6).

Fig. 8 Strain evolution in a one-way shape memory cycle for various levels of applied strain (A) and within a five-fold cyclic history at $\varepsilon_{appl} = 106\%$ (B); cycles carried out on PCL-high; the dashed segments in (A) represent the values of deformation applied before unloading (ε_{appl}).

Table 3 Strain fixity and strain recovery capabilities in the case of PCL-low

ε_{appl} (%)	Strain fixity^a (1st cycle) (%)	Strain recovery^b (1st cycle) (%)
45	100	100
60	100	100
125	100	100
225	100	96

^{a} Calculated according to eqn (2.5). ^{b} Calculated according to eqn (2.6).

cycle is displayed in Fig. 7 in terms of a strain–stress-temperature curve for an applied strain $\varepsilon_{appl} = 102\%$ on PCL-high. The specimen is first "programmed" to set a temporary shape, and this part of the cycle consists in heating the material at a deformation temperature, T_{def}, above T_m (step i, Fig. 7A and B; the pre-strain level, ε_0, is attained), deforming the material at a given level of applied strain, ε_{appl} (step ii; Fig. 7B and C) and cooling under fixed strain, after which the load is finally removed (step iii; Fig. 7C and D); no reliable values of the stress were measured in the cooling step, and for this reason in Fig. 7 this part of the curve is represented as a dashed line. After stress removal the residual strain at unloading (ε_{unload}) is measured and the strain reduction is further monitored during a heating ramp to temperatures above melting, until a final value of residual stress, ε_{rec}, is attained (step iv, D and E). On the values of ε_{unload} it was possible to evaluate the strain fixity (eqn (2.5)), while on those of ε_{rec} the strain recovery capabilities were determined (eqn (2.6)). In the cycle of Fig. 7 a high percentage of both strain fixity values (100% of the applied strain is permanently set after load removal) and strain recovery (98% of the applied strain is recovered through heating induced actuation) are found. The recovery process was mainly localized in
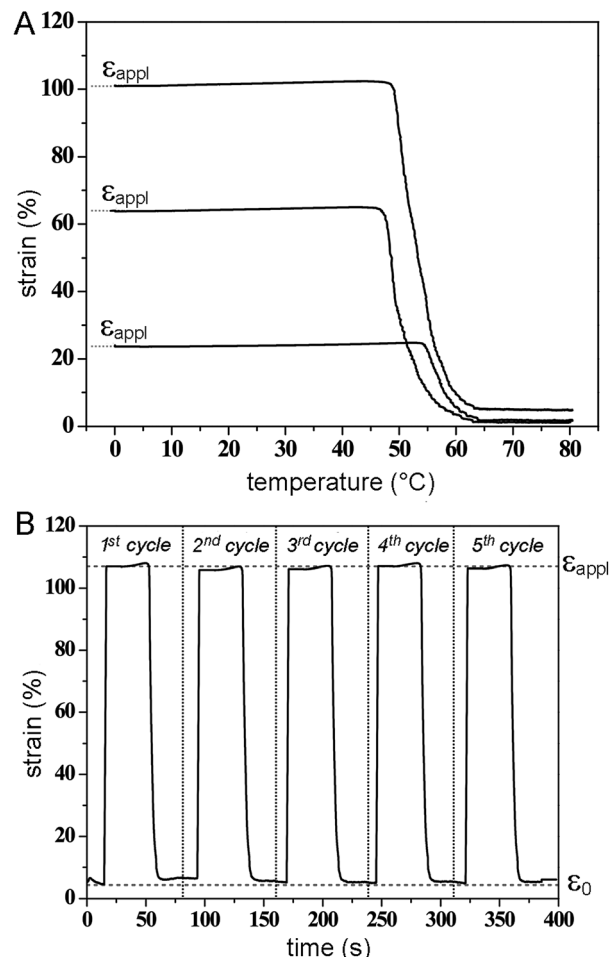
proximity of T_m, showing its steepest decrease at about 52 °C and an overall extent of the sigmoidal trend on a region between 50 °C and 65 °C.

The shape memory response was investigated also at further levels of strain and for more subsequent cycles. The results for PCL-high are summarized in terms of strain fixity and recovery in Table 2 and represented in terms of strain evolution in Fig. 8A, which reports the strain recovery for various ε_{appl}, and in Fig. 8B, which reports the strain recovery for five consecutive

cycles in case of $\varepsilon_{\text{appl}} = 106\%$. An overall similar recovery response is found for this material, independently from the strain level explored and the number of applied cycles.

The shape memory response of PCL-low was investigated on single shape memory cycles at various strain levels, in order to verify if the reduction in crosslinking density compromises the shape memory response. The thermo-mechanical response is practically the same as that of PCL-high, and the results are reported in Table 3 in terms of strain fixity and strain recovery.

High fixation and recovery capabilities are found at all the levels of strain explored, and only at the highest strain applied (225%) a slight reduction of the strain recovery to about 96% was found. The results show that also after this less extensive post-crosslinking treatment, the network structure developed is sufficient to still sustain large recovery capabilities. Other electrospun mats exploiting the T_{trans} of PCL reported in the literature[15,18,19] display very interesting shape memory properties, with good strain fixity and strain recovery values that, however, are overall lower than those reported in Tables 2 and 3 of the present work. For instance, the electrospun PDLCL fabrics described by Matsumoto and coworkers[18] exhibited good shape-memory properties with strain recovery of 89–95% and strain fixity of 82–83% after the 2nd cycle, when small deformations were applied at 60 °C. The UV-crosslinked PCL mat fabricated by Gong et al.[19] exhibited shape recover of 90% and shape fixity of 74.5%, after the 1st cycle, that were increased up to 92% and 83.7%, respectively, by the addition of MWNTs coated with Fe_3O_4. The SM mat described by Chen et al.[15] had a shape fixing of $99.1 \pm 0.4\%$ and a shape recovery of $81.3 \pm 0.8\%$ in the three cycles of the stretching-recovery test.

SEM analysis was carried out on PCL-high subjected to a single and five-fold shape memory cycle (Fig. 9A and B, respectively) at an applied strain of about 100% to evaluate changes in the fiber architecture after thermal activated recovery. The images show that shape recovery is accompanied by a recovery of the randomly oriented structures, also after the significant fiber alignment promoted by the applied strain (see Fig. 6D and F), and this finding is further confirmed by the close similarity of the 2-FFT plot of the recovered samples with that of the undeformed one, as shown in Fig. 9C.
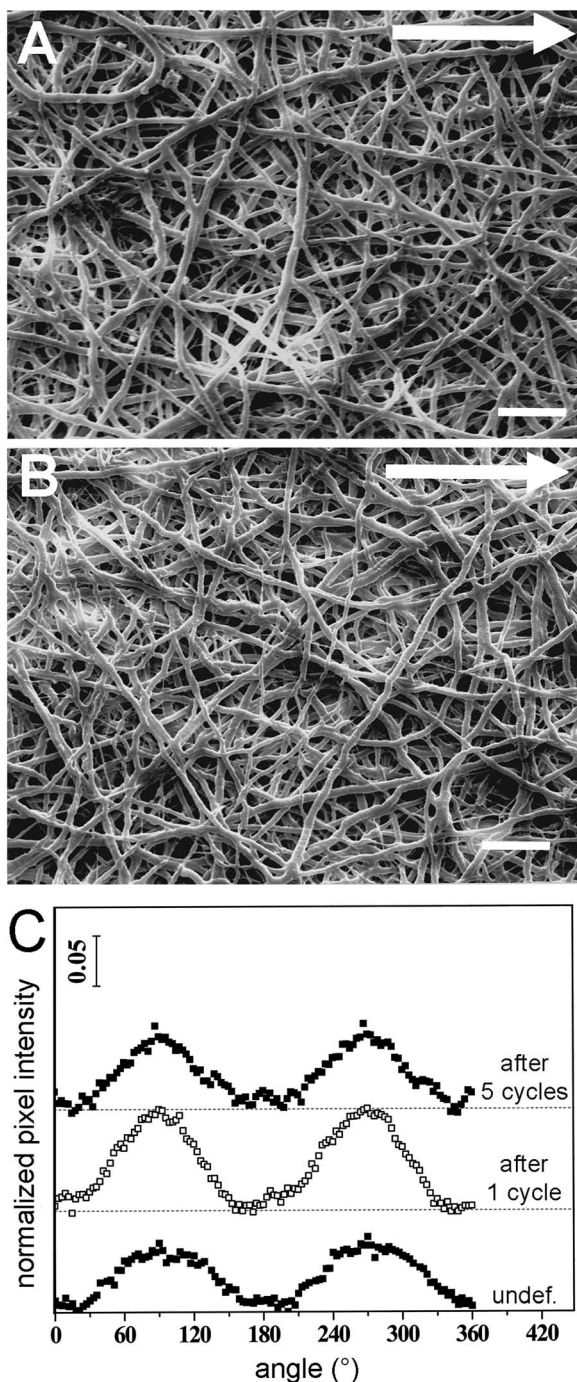

Fig. 9 SEM images of PCL-high subjected to a single (A) and five-fold (B) shape memory cycle at $\varepsilon_{\text{appl}} \simeq 100\%$ (the arrow indicates the strain direction); (C) comparison of the 2-D FFT plot of the undeformed and recovered specimens. Scale bars = 20 μm.

4. Conclusions

Partially crosslinked α,ω-triethoxysilane-terminated PCL solutions were successfully electrospun, allowing to obtain bead-free fibrous non-woven mats. The viscosity of the electrospinnable solution was optimized by controlling the hydrolysis/condensation reaction time activated by water and HCl, while the crosslinking degree of PCL fibers was controlled by varying the exposure time of non-woven mats to acidic vapors. The mechanical properties (storage modulus and tensile modulus) in the rubbery plateau region were consequently governed by the crosslinking degree of PCL. The evolution of fiber architecture within the non-woven mat with the applied strain was observed: the fibers underwent rotational/flexural motions, reorienting as the strain increases and, for strain values higher than 50% the fibers became highly stretched and aligned along the direction of strain. All the prepared electrospun non-woven mats exhibited very good one-way shape memory properties as evidenced by high fixation and recovery capabilities, almost independently on the applied strain and the crosslinking degree of PCL fibers. These results were obtained through a straightforward and facile process, without any need of polymeric

template or more complex approaches, obtaining a material with controllable ad adjustable crosslinking content.

Acknowledgements

Notes and references

1 A. Lendlein and S. Kelch, *Angew. Chem., Int. Ed.*, 2002, **41**, 2034–2057.

2 J. Hu, *Shape memory polymers and textiles*, Woodhead Publishing, Cambridge, 2007.

3 T. Xie, *Polymer*, 2011, **52**, 4985–5000.

4 C. M. Yakacki, R. Shandas, D. Safranski, A. M. Ortega, K. Sassaman and K. Gall, *Adv. Funct. Mater.*, 2008, **18**, 2428–2435.

5 M. Behl and A. Lendlein, *Mater. Today*, 2007, **10**, 20–28.

6 C. Liu, H. Qin and P. T. Mather, *J. Mater. Chem.*, 2007, **17**, 1543–1558.

7 A. Lendlein, M. Behl, B. Hiebl and C. Wischke, *Expert Rev. Med. Devices*, 2010, **7**, 357–379.

8 G. M. Baer, T. S. Wilson, W. Small, J. Hartman, W. J. Benett, D. L. Matthews and D. J. Maitland, *J. Biomed. Mater. Res., Part B*, 2009, **90**, 421–429.

9 L. Xue, S. Dai and Z. Li, *Biomaterials*, 2010, **31**, 8132–8140.

10 C. P. Buckley, C. Prisacariu and A. Caraculacu, *Polymer*, 2007, **48**, 1388–1396.

11 Q. Meng, J. Hu, Y. Zhu, J. Lu and Y. Liu, *J. Appl. Polym. Sci.*, 2007, **106**, 2515–2523.

12 Q. Meng, J. Hu and Y. Zhu, *J. Biomater. Sci., Polym. Ed.*, 2008, **19**, 1437–1454.

13 W. Wang, Y. Jin and Z. Su, *J. Phys. Chem. B*, 2009, **113**, 15742–15746.

14 B. Sun, Y. Z. Long, H. D. Zhang, M. M. Li, J. L. Duvail, X. Y. Jiang and H. L. Yin, *Prog. Polym. Sci.*, 2014, **39**, 862–890.

15 H. Chen, X. Cao, J. Zhang, J. Zhang, Y. Ma, G. Shi, Y. Ke, D. Tong and L. Jiang, *J. Mater. Chem.*, 2012, **22**, 22387–22391.

16 L. F. Tseng, P. T. Mather and J. H. Henderson, *Acta Biomater.*, 2013, **9**, 8790–8801.

17 M. Bao, X. Lou, Q. Zhou, W. Dong, H. Yuan and Y. Zhang, *ACS Appl. Mater. Interfaces*, 2014, **6**, 2611–2621.

18 H. Matsumoto, T. Ishiguro, Y. Konosu, M. Minagawa, A. Tanioka, K. Richau, K. Kratz and A. Lendlein, *Eur. Polym. J.*, 2012, **48**, 1866–1874.

19 T. Gong, W. Li, H. Chen, L. Wang, S. Shao and S. Zhou, *Acta Biomater.*, 2012, **8**, 1248–1259.

20 G. Chen, Y. Xu, D.-G. Yu, D.-F. Zhang, N. P. Chatterton and K. N. White, *Chem. Commun.*, 2015, **51**, 4623–4626.

21 D.-G. Yu, K. White, N. Chatterton, Y. Li, L. Lia and X. Wang, *RSC Adv.*, 2015, **5**, 9462–9466.

22 D.-G. Yu, X.-Y. Li, X. Wang, J.-H. Yang, S. W. A. Bligh and G. R. Williams, *ACS Appl. Mater. Interfaces*, 2015, **7**, 18891–18897.

23 K. Paderni, S. Pandini, S. Passera, F. Pilati, M. Toselli and M. Messori, *J. Mater. Sci.*, 2012, **47**, 4354–4362.

24 R. L. Miller, *Crystallographic data for various polymers In:Polymer Handbook*, John Wiley & Sons, New York, 3rd end, 1992.

25 C. E. Ayres, B. S. Jha, H. Meredith, J. R. Bowman, G. L. Bowlin, S. C. Henderson and D. G. Simpson, *J. Biomater. Sci., Polym. Ed.*, 2008, **19**, 603–621.

26 S. L. Shenoy, W. D. Bates, H. L. Frisch and G. E. Wnek, *Polymer*, 2005, **46**, 3372–3384.

27 M. G. McKee, G. L. Wilkes, R. Colby and T. E. Long, *Macromolecules*, 2004, **37**, 1760–1767.

28 R. H. Colby, L. J. Fetters, W. G. Funk and W. W. Graessley, *Macromolecules*, 1991, **24**, 3873–3882.

29 S. L. Shenoy, W. D. Bates and G. E. Wnek, *Polymer*, 2005, **46**, 8990–9004.

30 S. Pandini, F. Baldi, K. Paderni, M. Messori, M. Toselli, F. Pilati, A. Gianoncelli, M. Brisotto, E. Bontempi and T. Riccò, *Polymer*, 2013, **54**, 4253–4265.

31 R. Inai, M. Kotaki and S. Ramakrishna, *J. Polym. Sci., Part B: Polym. Phys.*, 2005, **43**, 3205–3212.

32 X. Wei, Z. Xia, S.-C. Wong and A. Baji, *Int. J. Exp. Comput. Biomech.*, 2009, **1**, 45.

33 F. Zhang, Z. Zhang, Y. Liu and J. Leng, *Fibers Polym.*, 2014, **15**, 534–539.